THE JOURNAL OF BIOLOGICAL CHEMISTRY VOL. 285, NO. 48, pp. 37370–37376, November 26, 2010

Ca^{2+} Overload and Sarcoplasmic Reticulum Instability in *tric-a* Null Skeletal Muscle*[S]

Received for publication, July 29, 2010, and in revised form, September 13, 2010 Published, JBC Papers in Press, September 21, 2010, DOI 10.1074/jbc.M110.170084

Xiaoli Zhao[‡1], Daiju Yamazaki[§], Ki Ho Park[‡], Shinji Komazaki[¶], Andoria Tjondrokoesoemo[‡], Miyuki Nishi[§], Peihui Lin[‡], Yutaka Hirata[‡‖], Marco Brotto[**], Hiroshi Takeshima[§], and Jianjie Ma[‡2]

*From the [‡]Department of Physiology and Biophysics, Robert Wood Johnson Medical School, Piscataway, New Jersey 08854, the [§]Department of Biological Chemistry, Graduate School of Pharmaceutical Sciences, Kyoto University, Kyoto 606-8501, Japan, the [¶]Department of Anatomy, Saitama Medical University, Saitama 350-0495, Japan, the [‖]Division of Physiome, Department of Physiology, Hyogo College of Medicine, Hyogo 663-8501, Japan, and the **Department of Nursing and Medicine, University of Missouri, Kansas City, Missouri 64108*

The sarcoplasmic reticulum (SR) of skeletal muscle contains K^+, Cl^-, and H^+ channels may facilitate charge neutralization during Ca^{2+} release. Our recent studies have identified trimeric intracellular cation (TRIC) channels on SR as an essential counter-ion permeability pathway associated with rapid Ca^{2+} release from intracellular stores. Skeletal muscle contains TRIC-A and TRIC-B isoforms as predominant and minor components, respectively. Here we test the physiological function of TRIC-A in skeletal muscle. Biochemical assay revealed abundant expression of TRIC-A relative to the skeletal muscle ryanodine receptor with a molar ratio of TRIC-A/ryanodine receptor ~5:1. Electron microscopy with the *tric-a*$^{-/-}$ skeletal muscle showed Ca^{2+} overload inside the SR with frequent formation of Ca^{2+} deposits compared with the wild type muscle. This elevated SR Ca^{2+} pool in the *tric-a*$^{-/-}$ muscle could be released by caffeine, whereas the elemental Ca^{2+} release events, *e.g.* osmotic stress-induced Ca^{2+} spark activities, were significantly reduced likely reflecting compromised counter-ion movement across the SR. *Ex vivo* physiological test identified the appearance of "alternan" behavior with isolated *tric-a*$^{-/-}$ skeletal muscle, *i.e.* transient and drastic increase in contractile force appeared within the decreasing force profile during repetitive fatigue stimulation. Inhibition of SR/endoplasmic reticulum Ca^{2+} ^{ATPase} function could lead to aggravation of the stress-induced alternans in the *tric-a*$^{-/-}$ muscle. Our data suggests that absence of TRIC-A may lead to Ca^{2+} overload in SR, which in combination with the reduced counter-ion movement may lead to instability of Ca^{2+} movement across the SR membrane. The observed alternan behavior with the *tric-a*$^{-/-}$ muscle may reflect a skeletal muscle version of store overload-induced Ca^{2+} release that has been reported in the cardiac muscle under stress conditions.

In skeletal muscle, transient elevation of intracellular Ca^{2+} causes muscle contraction upon depolarization of the plasma membrane that leads to opening of the ryanodine receptor (RyR)[3]/Ca^{2+} release channel on the sarcoplasmic reticulum (SR) in a process termed excitation-contraction (E-C) coupling (1–3). Efficient operation of E-C coupling in skeletal muscle requires a number of cellular components: first, the junctional structure between SR and transverse tubular invagination of the plasma membrane must be maintained for efficient signal transduction from membrane depolarization to RyR channel opening (4, 5); second, an optimal environment must be preserved in the cytosol to maintain the RyR channel in a functional state; and third, ion homeostasis inside the SR lumen must be adjusted to accommodate the rapid efflux of Ca^{2+} out of the SR, as Ca^{2+} efflux will establish a transient negative potential inside the SR. This negative potential, if not balanced, will impede Ca^{2+} release and slow down the regenerative aspect of the intracellular Ca^{2+} signaling.

In the course of searching for membrane proteins participating in E-C coupling of striated muscle, we identified two isoforms of trimeric intracellular cation (TRIC) channel that were specifically expressed in the SR membrane (6). TRIC-A is preferentially expressed in striated muscles and TRIC-B is ubiquitously present in most mammalian tissues. Purified TRIC-A and TRIC-B protein formed K^+-permeable channels in lipid bilayer membrane with distinct pharmacological characteristics (6, 7), and share properties of the native SR K^+ channels reported by Coronado and Miller (8).

Although *tric-a*$^{-/-}$ mice are apparently normal and could reach adulthood, the *tric-a*$^{-/-}$*tric-b*$^{-/-}$ double knock-out mice die at E9.5 day due to cardiac arrest (6), whereas the *tric-b*$^{-/-}$ neonates die shortly after birth due to respiratory failure (9). Considering the distinct tissue-distributing pattern of TRIC-A and TRIC-B and the different modulatory functions of the TRIC-A and TRIC-B channels (7), it is likely that these two isoforms have different physiological functions in different organs. Because skeletal muscle has the most abundant expres-

* This work was supported, in whole or in part, by National Institutes of Health Grant RO1-AG28856 (to J. M. and H. T.), grants from the Takeda Science Foundation (to H. T.), an American Heart Association National Scientist Development grant (to X. Z.), and the Nagai Foundation of Tokyo (to D. Y.).

[S] The on-line version of this article (available at http://www.jbc.org) contains supplemental Figs. S1 and S2.

[1] To whom correspondence may be addressed. Tel.: 732-235-4474; E-mail: zhaox1@umdnj.edu.

[2] To whom correspondence may be addressed. Tel.: 732-235-4494; E-mail: maj2@umdnj.edu.

[3] The abbreviations used are: RyR, ryanodine receptor; CSQ, calsequestrin; CPA, cyclopiazonic acid; E-C, excitation-contraction coupling; EDL, extensor digitorium longus; FDB, flexor digitorum brevis; SR, sarcoplasmic reticulum; SERCA, sarcoplasmic/endoplasmic reticulum Ca^{2+}-ATPase; TRIC, trimeric intracellular cation; BES, 2-[bis(2-hydroxyethyl)amino]ethanesulfonic acid.

sion of TRIC-A, TRIC-A may play a more important role in skeletal muscle.

In this study, we examine the physiological function of TRIC-A in Ca^{2+} signaling of skeletal muscle. We show that TRIC-A is expressed in the SR membrane of skeletal muscle at a high molecular ratio to RyR. Genetic ablation of TRIC-A leads to SR vacuolization and Ca^{2+} overload in skeletal muscle. In the absence of TRIC-A-mediated K^+ permeability, chronic SR Ca^{2+} overload creates instability for Ca^{2+} movement across the SR membrane, which leads to the appearance of "mechanical alternans" in the mutant muscle under stress conditions, a phenotype that can be aggravated by the sarcoplasmic/endoplasmic reticulum Ca^{2+}-ATPase (SERCA) inhibitor. Our data suggests that TRIC-A contributes to ion movement across SR and is an important component of the E-C coupling machinery in skeletal muscle.

MATERIALS AND METHODS

Animals—Wild type rabbits (Japanese white, 3 kg) were used for microsome isolation from the hindlimb. 3–4-Month-old wild type or *tric-a*$^{-/-}$ male mice of the same genetic background (F1:J1 embryonic stem cells × C57BL/6J) were used for all other experiments.

Microsome Protein Profiling—Total microsome were prepared from rabbit skeletal muscle as previously described (10) and solubilized in buffer containing 1% *N*-dodecyl-β-D-maltoside, 0.25 M sucrose, 2 mM 2-mercaptoethanol, 50 mM Tris-HCl (pH 7.4), and protease inhibitors. Microsomal fraction were separated on 10% SDS-PAGE electrophoresis along with bovine serum albumin (BSA) and stained by Coomassie Brilliant Blue solution (Nacalai, Kyoto, Japan). Protein concentrations were determined by comparing relative density of the target protein with BSA after Coomassie Brilliant Blue staining.

Western Blotting—Total cellular protein was extracted from hindlimb, extensor digitorum longus (EDL), and soleus of wild type and *tric-a*$^{-/-}$ mice in a buffer containing 0.3 M sucrose, 20 mM Tris-HCl (pH 7.4) and protease inhibitors. 10 μg of protein were loaded on 12% SDS-PAGE and transferred onto a polyvinylidene difluoride membrane. Antibodies used were polyclonal rabbit antibody against TRIC-A, polyclonal antibody against TRIC-B, mouse monoclonal antibody against RyR (Affinity Bioreagents), rabbit polyclonal antibody against Junctophilin-1, rabbit polyclonal antibody against Na^+-Ca^{2+} exchanger 1 (gift from Dr. Iwamoto), mouse monoclonal antibody against Na^+-Ca^{2+} exchanger 3 (gift from Dr. Iwamoto), rabbit polyclonal antibody against calsequestrin 1 (CSQ1), mouse monoclonal antibody against sarcomeric α-actin (Sigma), and goat anti-rabbit secondary antibody.

Oxidized Iron Staining Electron Microscopy (EM)—EDL, soleus, and flexor digitorum brevis (FDB) muscles were dissected from mice and embedded overnight in pre-fixative solution (3% paraformaldehyde, 2.5% glutaraldehyde, 0.1 M cacodylate buffer, pH 7.5) containing 0.1 M potassium oxalate. After brief washing with 0.1 M cacodylate buffer, samples were placed in post-fixative solution (0.1% OsO_4, 0.1 M potassium ferricyanide, and 0.1 M cacodylate buffer, pH 7.4) and fixed for 2 h at room temperature. Then, samples were washed briefly with the same buffer, dehydrated using ethanol/acetone, and embedded in epoxy resin. Thick sections (150–200 nm) were cut and observed without uranyl acetate and lead citrate staining. Slides were examined under a JEOL-1010 transmission electron microscope. 223 muscle cells on average were examined in each sample and the percentage of vacuolization containing electron dense Ca^{2+} deposit in each sample was calculated.

Measurement of Caffeine-induced Ca^{2+} Transient and Osmotic-induced Ca^{2+} Sparks—FDB fibers were isolated by enzymatic disassociation in 2 mg/ml of type I collagenase (Sigma) and loaded with either 10 μM Fura-2 AM (Invitrogen) for measurement of caffeine-induced Ca^{2+} transient and 10 μM Fluo-4-AM for osmotic-induced Ca^{2+} spark for 1 h at room temperature. Fibers were then washed by 2.5 mM Tyrode solution (in mM, 140 NaCl, 5 KCl, 10 Hepes, 2.5 $CaCl_2$, 2 $MgCl_2$, pH 7.2). Measurement of caffeine-induced Ca^{2+} transient was performed on microscopic system of a PTI spectrofluorometer (Photon Technology International, Princeton, NJ), and changes in $[Ca^{2+}]_i$ were determined as changes in the ratio of Fura-2 fluorescence at excitation wavelengths of 350 and 380 nm, following exposure to 20 mM caffeine in Tyrode solution without Ca^{2+}.

Measurements of Ca^{2+} spark were performed on a confocal microscope (Radiance 2100, Bio-Rad) (11). Fibers were first stabilized in 2.5 mM Tyrode solution, then perfused with a 170 mosM hypotonic solution containing (in mM) 70 NaCl, 5 KCl, 10 Hepes, 2.5 $CaCl_2$, 2 $MgCl_2$, pH 7.2, for 60–180 s to induce swelling before perfusion was switched back to the initial 2.5 mM Tyrode solution with an osmolarity of 290 mosM. Spark events were caught on a line scan at a sampling rate of 2 ms per line and image analysis was performed using custom routines on IDL software (Research Systems, Inc.). All experiments were conducted at room temperature (23 ± 2 °C).

Measurement of Membrane Potential—SR vesicles were prepared from 3–6-month-old mice as described previously (10). SR vesicles containing 60 g of protein were resuspended in 2 ml of Cl^--free SR-loading buffer (in mM: K glutamate 107.8, EGTA-KOH 2, $MgSO_4$ 6.6, ATP 5.4, creatine phosphate 15, Ca^{2+} gluconate 0.98, BES-KOH 20, pH 7.2, free Ca^{2+} level of pCa = 6.6), supplemented with 0.5 M di-8-ANEPPQ (Invitrogen) for 6 min at room temperature with constant stirring. Potential dependent fluorescence changes in response to 40 μM A23187 or 0.2% Triton X-100 were monitored in a DeltaRAM fluorometer (Photon Technology International) with an emission wavelength of 570 nm and a ratio of the excitation intensity of F_{510}/F_{450}.

Contractility of Isolated Muscles—As previously described (12), intact EDL and soleus muscle bundles were dissected from wild type and *tric-a*$^{-/-}$ mice and mounted in Radnotti glass chambers with built-in platinum stimulating electrodes (Monrovia, CA), bathing in 2.5 mM Ca^{2+} Tyrode solution with 10 mM glucose, saturated with 100% O_2. One tendon of the muscle was attached to a force transducer and the other one to a stationary arm. A Powerlab computer interface program (ADInstruments) was used to control the electrical stimulation protocols. Muscles were adjusted to produce maximal isometric force and equilibrated at 80 Hz for 30 min (1-min interval, 0.83% duty cycle) using squared-wave 300-mA electrical currents of 500-ms duration. Contractile force at a range of frequencies

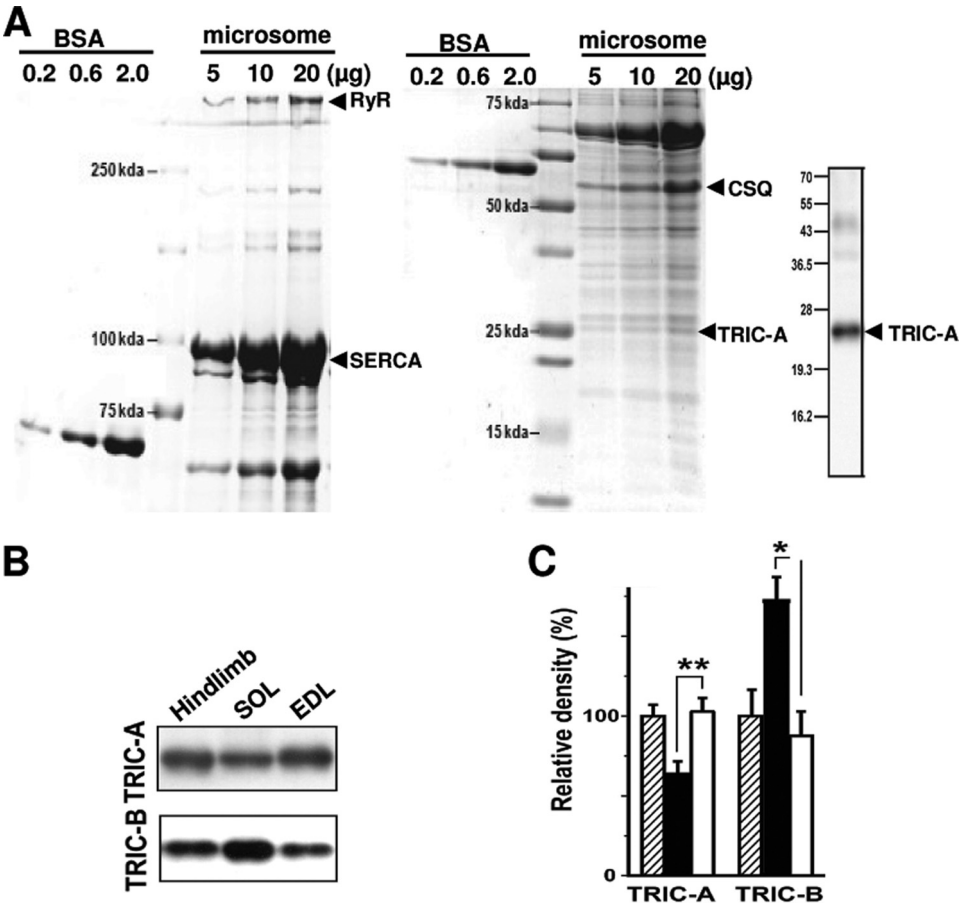

FIGURE 1. **Abundant expression of TRIC protein in skeletal muscles.** *A*, representative Coomassie Brilliant Blue staining showed the relative expression levels of RyR (552 kDa) and SERCA protein (100 kDa) (*left panel*), as well as CSQ (60 kDa) and TRIC-A protein (33 kDa) (*middle panel*) in isolated SR microsome from rabbit skeletal muscle, as compared with the BSA standard. *Right panel* was a Western blot of the isolated microsome from rabbit hindlimb skeletal muscle using rabbit polyclonal anti-TRIC-A antibody. *B*, representative Western blot showing the differential expression patterns of TRIC-A and TRIC-B in hindlimb, soleus (*SOL*), and EDL from the wild type mice. *C*, summarized data of the relative expression levels of TRIC-A and TRIC-B in hindlimb ($n = 8$), soleus ($n = 8$), and EDL ($n = 8$) from wild type skeletal muscle. The expression levels of TRIC-A and TRIC-B in hindlimb were set as 100%, **, $p < 0.01$.

were tested including 1, 5, 10, 20, 30, 40, 50, 60, 80, 100, 120, 140, and 160 Hz, and the maximal force (T_{max}) was identified. Muscles were then exposed to a fatiguing stimulation protocol (1-s interval, 50% duty cycle) using the 50% T_{max} stimulation for 5 min. Mechanical alternans in *tric-a* null muscles were induced by 3 repeated fatiguing protocols, with a 20-min recovery period at 50% T_{max} stimulation between, but alternans can be seen in the first, second, or the last fatiguing process.

For testing the presence of alternans with SERCA inhibition, cyclopiazonic acid (CPA) (Sigma) was added to the bathing solution in a final concentration of 20 μM for 5 min and intact EDL and soleus muscles were subjected to fatigue stimulation at 20 Hz, followed by 60 Hz fatigue stimulation after a 5-min break. Alternans in either the first or second fatiguing process were counted.

Characterization of tric-$a^{-/-}$ Mice at Whole Animal Level—Body weight of the male and female mice was measured biweekly from week 2 after birth to week 20. At 12 weeks old, wild type and *tric-$a^{-/-}$* mice were subjected to a graded running exercise beginning at 10 m/min and increased by 2 m/min every 2 min on a rodent treadmill. The session was terminated when the mice refused to run and maximal speed was recorded. In addition, wild type and *tric-$a^{-/-}$* mice were placed on a rod rotating at 28 rpm and retention time on the rod was recorded. Maximum of 120 s was allowed for one rota-rod trial.

Statistics—All data were analyzed by Origin software (OriginLab). Values are mean ± S.E. Significance was determined by Student's *t* test. A value of $p < 0.05$ was used as criteria for statistical significance and other *p* values were as specified in the figure legends.

RESULTS AND DISCUSSION

We identified TRIC-A through an immuno-proteomic approach using monoclonal antibodies against the skeletal muscle triad junction proteins (13). Our initial study has established TRIC-A as a K^+-permeable channel in the SR membrane and its role in supporting RyR-mediated Ca^{2+} release in both cardiac and skeletal muscles (6). A more recent study revealed the essential role of TRIC-B in Ca^{2+} handling of alveolar epithelial cells and in perinatal lung development and maturation (9). Specifically, *tric-$b^{-/-}$* epithelial cells displayed compromised inositol 1,4,5-trisphosphate receptor-mediated intracellular Ca^{2+} release even though Ca^{2+} overload was present in the endoplasmic reticulum. Because TRIC-A and TRIC-B have different biophysical properties (7), these two channels likely have distinct roles in regulating intracellular Ca^{2+} signaling in both excitable and non-excitable cells.

Embryonic lethality associated with the *tric-a* and *tric-b* double knock-out mice prevented our physiological evaluations of TRIC-A and TRIC-B in adult muscle tissues. Fortunately, the *tric-$a^{-/-}$* mice are viable and appear normal under non-stress conditions, for example, our observation revealed that *tric-$a^{-/-}$* mice had normal growth rate and mobility at the whole animal level (supplemental Fig. S1). So we set off to investigate the physiological role of TRIC-A in skeletal muscle under stress conditions in the current study. Toward defining the function of TRIC-A in skeletal muscle, microsome preparations isolated from rabbit skeletal muscle was used to quantify the relative expression level of TRIC-A to other major Ca^{2+} regulatory proteins present in the SR (*e.g.* RyR, CSQ, and SERCA) (Fig. 1*A*). Molecular identities of the corresponding proteins were confirmed by Western blot for TRIC-A (Fig. 1*A*) and CSQ, RyR, and SERCA (not shown). As shown in Table 1, RyR is present in

the rabbit skeletal microsome preparation at 16.3 ± 1.4 pmol/mg, and TRIC-A is present at 89 ± 11 pmol/mg. Assuming tetramers of RyR are required for a functional Ca^{2+} release channel (14), and trimers of TRIC-A are required for a functional K^+ channel (6), these numbers would lead to a molecular ratio of ~5 to 1 for TRIC-A/RyR. Our method used to quantify the protein levels for RyR, SERCA, and CSQ is comparable with previous reports by other investigators (15, 16). The abundant expression of TRIC-A in skeletal muscle is consistent with the function as a countercurrent channel for RyR Ca^{2+} release, as a redundancy may be necessary to support the repeated Ca^{2+} release events from the SR.

TABLE 1

Relative expression level of TRIC-A to other SR resident proteins

Protein contents of RyR (tetramer), SERCA, CSQ, and TRIC-A (trimer) in isolated microsome from rabbit skeletal muscle were summarized in this table. Values were mean ± S.E. (μg/mg microsome) and $n = 4$. Functional unit (pmol/mg of microsome) was calculated by the formula: protein content/(molecular weight × reported subunit numbers). Reported contents of RyR and SERCA (pmol/mg) in microsome from two other groups were included as a reference.

	Protein content	Functional unit	Reported content
	μg/mg microsome	*pmol/mg microsome*	
RyR (tetramer)	36.6 ± 3.2	16.3 ± 1.4	8–20
SERCA	367 ± 37	3,480 ± 350	3,000–4,000
CSQ	41.0 ± 2.0	680 ± 33	
TRIC-A (trimer)	8.8 ± 1.1	89 ± 11	

Using immunoblot assays, we found that in addition to TRIC-A, TRIC-B is also present in skeletal muscle (Fig. 1*B*). Both the fast-twitch EDL muscle and the slow-twitch soleus muscle contain TRIC-A and TRIC-B proteins, but at different concentrations (Fig. 1*C*). Genetic ablation of TRIC-A did not appear to affect the expression level of TRIC-B, because similar levels of TRIC-B expression were detected in the wild type and *tric-a*$^{-/-}$ muscles (supplemental Fig. S2), supporting that TRIC-A and TRIC-B may have complementary functions in Ca^{2+} signaling in muscle tissues. In addition, other major Ca^{2+} regulatory proteins in the *tric-a*$^{-/-}$ muscle also showed a similar expression pattern as the wild type control muscle (supplemental Fig. S2), suggesting that germ-line ablation of *tric-a* did not lead to significant changes in the overall Ca^{2+} signaling machinery in skeletal muscle.

Systemic ablation of *tric-a* did not appear to affect development of the mice, significant changes in the ultrastructure of the SR network and Ca^{2+} handling properties inside the SR organelle were observed through electron microscopy (EM) (Fig. 2). Specifically, using fixative solution supplemented with potassium oxalate and potassium ferricyanide ($K_3Fe(CN)_6$) to visualize concentrated Ca^{2+} deposits in intracellular organelles, we detected frequent SR vacuolization and Ca^{2+} deposits in the *tric-a* knock-out EDL and soleus muscles by EM. Ca^{2+} deposition could be detected only in large-sized SR vacuoles from the *tric-a*$^{-/-}$ muscles, confirmed by transmission EM oxidized iron staining images (Fig. 2, *B–E*). These phenomena were rarely observed in skeletal muscle derived from the wild type controls (Fig. 2*A*). Summary data for the presence of vacuoles in wide type and *tric-a*$^{-/-}$ muscles were summarized in Table 2. The slightly higher basal level of vacuolization in the fast-twitch muscle may reflect the less oxidative capacity of these muscles to endure the anaerobic environment during sample preparation. These structural defects with the adult *tric-a*$^{-/-}$ skeletal muscle were similar to what we observed previously with the *tric-a*$^{-/-}$*tric-b*$^{-/-}$ neonates, which showed frequent formation of Ca^{2+} deposits and overload of Ca^{2+} inside the SR of the embryonic cardiomyocytes (6).

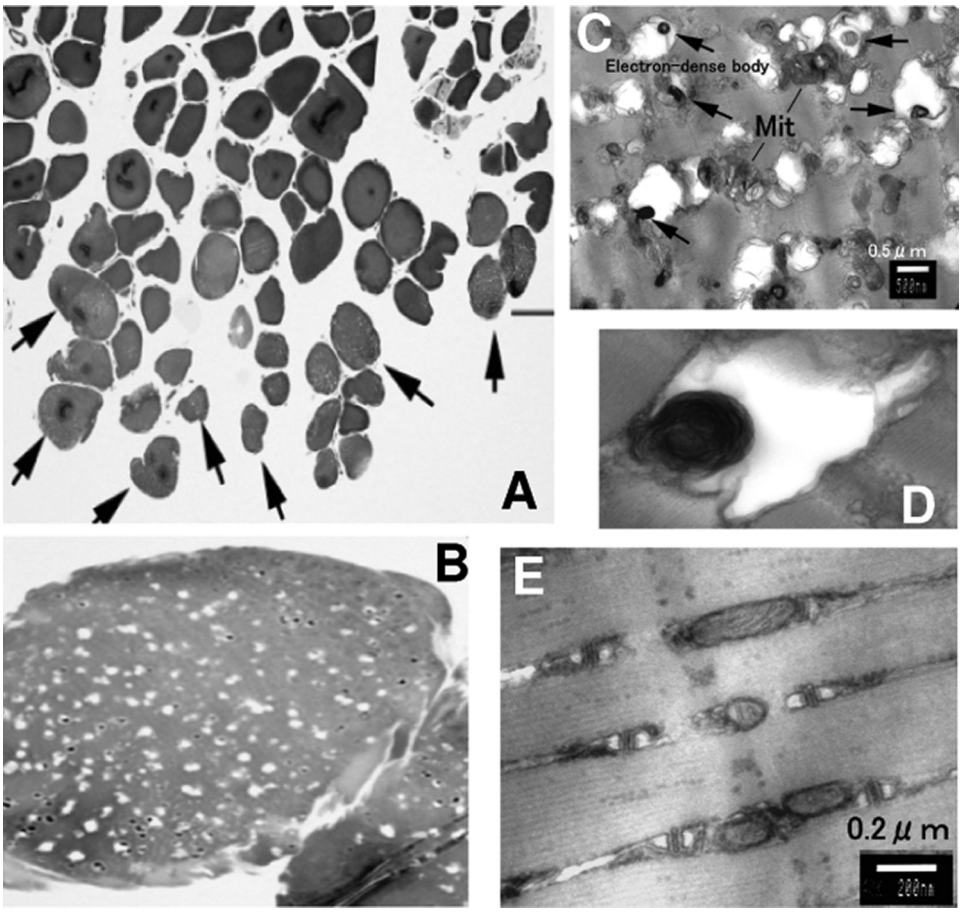

FIGURE 2. **Detection of large-size vacuoles containing electron-dense Ca^{2+} deposit in *tric-a*$^{-/-}$ muscles.** *A*, toluidine blue-stained light microscopic cross-section image of a *tric-a*$^{-/-}$ muscle bundle at low magnification, *arrows* designate myofibrils containing large-sized vacuoles. *B*, enlarged image of a single *tric-a*$^{-/-}$ myofibril containing large-sized vacuoles. *C*, transmission EM image stained by oxidized iron showed the longitudinal thick section of *tric-a*$^{-/-}$ FDB at high magnification. Mitochondria (*Mit*) was labeled in the image and *arrows* designate electron dense Ca^{2+} deposits in the large-sized vacuoles (>0.5 μm in diameter), preferentially formed in the terminal SR region. *D*, enlarged image showing a Ca^{2+}-overloaded swollen SR. *E*, transmission EM image stained by oxidized iron showed the longitudinal thick section of wild type FDB at high magnification.

TABLE 2

Increased large-size vacuolization containing Ca^{2+} deposit in *tric-a*$^{-/-}$ muscles

The incidence of large-sized vacuoles (%) in wild type and *tric-a*$^{-/-}$ skeletal muscles were calculated and compared. Data shown are mean ± S.E. Fast-twitch muscles included 4 pairs of EDL and 4 pairs of FDB, whereas slow-twitch muscle included 4 pairs of soleus.

Large vacuoles (%)	Wild type	*tric-a*$^{-/-}$
Fast-twitch muscles ($n = 8$)	0.64 ± 0.26	6.18 ± 2.42[a]
Slow-twitch muscles ($n = 4$)	0.25 ± 0.25	11.13 ± 4.56[a]

[a] $p < 0.05$ compared with wild type.

We used caffeine to test if the total RyR-mediated Ca^{2+} releasable pool from the SR was altered with the *tric-a*$^{-/-}$ skeletal muscle. As shown in Fig. 3*A*, application of 20 mM caffeine evoked a significantly larger Ca^{2+} transient in the *tric-a*$^{-/-}$ muscle fiber as compared with the wild type fiber. This result is consistent with the increased Ca^{2+} deposit detected with EM, and similar to our previous study with the embryonic cardiac cells (6) and neonatal epithelial cells (9).

Our previous studies show that transient osmotic stress applied to the adult skeletal muscle can uncover fluttered Ca^{2+} spark events from the SR (11). Using this methodology, we identified significant defects in Ca^{2+} spark signaling in the *tric-a*$^{-/-}$ muscle (Fig. 3*B*). The frequency of Ca^{2+} sparks was significantly reduced in the *tric-a*$^{-/-}$ muscle (Fig. 3*C*). Although the amplitude of Ca^{2+} sparks was not significantly reduced in the mutant muscle as compared with the wild type fibers, taking into account that *tric-a*$^{-/-}$ muscle fiber had a significantly larger releasable SR Ca^{2+} pool (Fig. 3*A*), it suggests that the Ca^{2+} mobilization process through the RyR channel is compromised due to lack of the TRIC-A-based counter-ion current. The duration of Ca^{2+} spark events seemed to increase in the *tric-a*$^{-/-}$ fibers, possibly reflecting a compromised mechanism of Ca^{2+}-dependent RyR inactivation.

The compromised Ca^{2+} spark signaling associated with knock-out of the *tric-a* gene may correlate with changes in TRIC-A-mediated membrane permeability across the SR. To test this possibility, we used the voltage-sensitive fluorescent dye di-8-ANEPPQ to probe the membrane potential of SR vesicles isolated from *tric-a*$^{-/-}$ and wild type mice. As shown in Fig. 3*D*, isolated *tric-a*$^{-/-}$ SR vesicles displayed a significantly more negative potential at the cytosolic side as compared with the wild type control, which could be eliminated using Ca^{2+} ionophore A23187, suggesting correlation between the altered SR membrane potential to the increased Ca^{2+} content inside the SR. Overall, our data in Fig. 3 revealed the following aspects with the *tric-a*$^{-/-}$ muscle: first, there is overload of Ca^{2+} inside the SR; second, there are defects in membrane permeability across the SR membrane. The absence of TRIC-A-mediated K^+ permeability is likely the cause for the compromised Ca^{2+} spark signaling in the mutant mice.

Consequences of these ion mobilization defects on performance of the *tric-a*$^{-/-}$ muscle was revealed in our *ex vivo* muscle fatigability assays. Intact muscle bundles were subjected to repeated electrical stimulations to induce fatigue. As shown in Fig. 4*A*, the fatigue stimulation usually causes the contractile force in wild type muscle to decline exponentially. However, in *tric-a* knock-out muscle, the continuous force decay was interrupted by a sudden, transient increase in the contractile force generated, similar to the alternans described in myocardium (Fig. 4*B*). Although the alternans seen in skeletal muscle are of a more irregular nature, we gave these spikes of contractile forces a descriptive name, *i.e.* mechanical alternans. Our definition of a mechanical alternan is such that the contractile force outbreak has to be 50% higher than its previous force and the outbreaks should be seen at least 10 times during the 5-min fatigue stimulation process. Accordingly, the frequency of mechanical alternans in wild type was 0% for both EDL and soleus muscles, whereas that in *tric-a* knock-out muscles were 31 and 39%, respectively. To test whether the mechanical alternans were due to damage to the muscle fibers, we compared the force recovery percentage after fatigue stimulation in both wild type and *tric-a*$^{-/-}$ muscle bundles. The mutant muscle fibers showed similar force recovery rate for both fast-twitch and slow-twitch muscle bundles (0.67 ± 0.04 for EDL and 0.73 ± 0.07 for soleus) as the wild type controls (0.74 ± 0.05 for EDL and 0.85 ± 0.03 for soleus, all $p > 0.05$), suggesting that the stress-induced mechanical alternans are not due to changes in contractile machinery of the *tric-a*$^{-/-}$ muscle.

Alternans were first discovered in cardiomyocytes (17–20), which are closely correlated to both Ca^{2+} cycling and mechanical beat of the heart (21). Altered coupling between RyR-mediated intracellular Ca^{2+} release and various mechanisms of Ca^{2+} movement across the sarcolemmal membrane, including L-type Ca^{2+} channel and Na^+/Ca^{2+} exchanger, may underlie the alternan behavior in cardiac muscle (22). In particular, stress-induced SR Ca^{2+} overload can lead to occurrence of spontaneous extra-systole due to store overload-induced Ca^{2+} release (23), and cardiac RyR channels contain the intrinsic regulatory mechanisms for store overload-induced Ca^{2+} release. Thus, we speculate that the mechanical alternans observed in the *tric-a* knock-out skeletal muscle may represent instability of the SR Ca^{2+} release machinery due to overload of the SR Ca^{2+} store and reduced membrane permeability for K ions. It is worth noting that although the skeletal RyR/Ca^{2+} release channel is less sensitive to store overload-induced Ca^{2+} release (24), it may be activated under repetitive fatiguing stimulations.

To further test the contribution of SR Ca^{2+} transport to the stress-induced alternans in the *tric-a*$^{-/-}$ muscle, we added 20 μM CPA, a potent and reversible SERCA inhibitor (25) into the bath solution. Addition of CPA leads to the appearance of a slow-relaxing component of the contractile fore (80 Hz stimulation) in the wild type muscle (Fig. 4*C*, *top panel*), as expected for the reduced SERCA activity (26). Interestingly, in the presence of CPA, fatigue stimulation of the wild type muscle led to the appearance of mild alternan behavior (Fig. 4*C*, *bottom panel*, 4 of 10 muscle preparations). More importantly, CPA inhibition of SERCA function could aggravate the alternan behavior in the *tric-a*$^{-/-}$ muscle, because more drastic and more frequent alternan events (8 of 10) were observed under such experimental conditions (Fig. 4*D*, *lower panel*). This data provides direct evidence that altered SR Ca^{2+} transport is associated with the stress-induced alternans in the *tric-a*$^{-/-}$ muscle, and further suggest that ablation of TRIC-A could lead to instability of Ca^{2+} transport across the SR membrane.

In summary, our study demonstrated the important physiological function of TRIC-A in Ca^{2+} signaling of skeletal

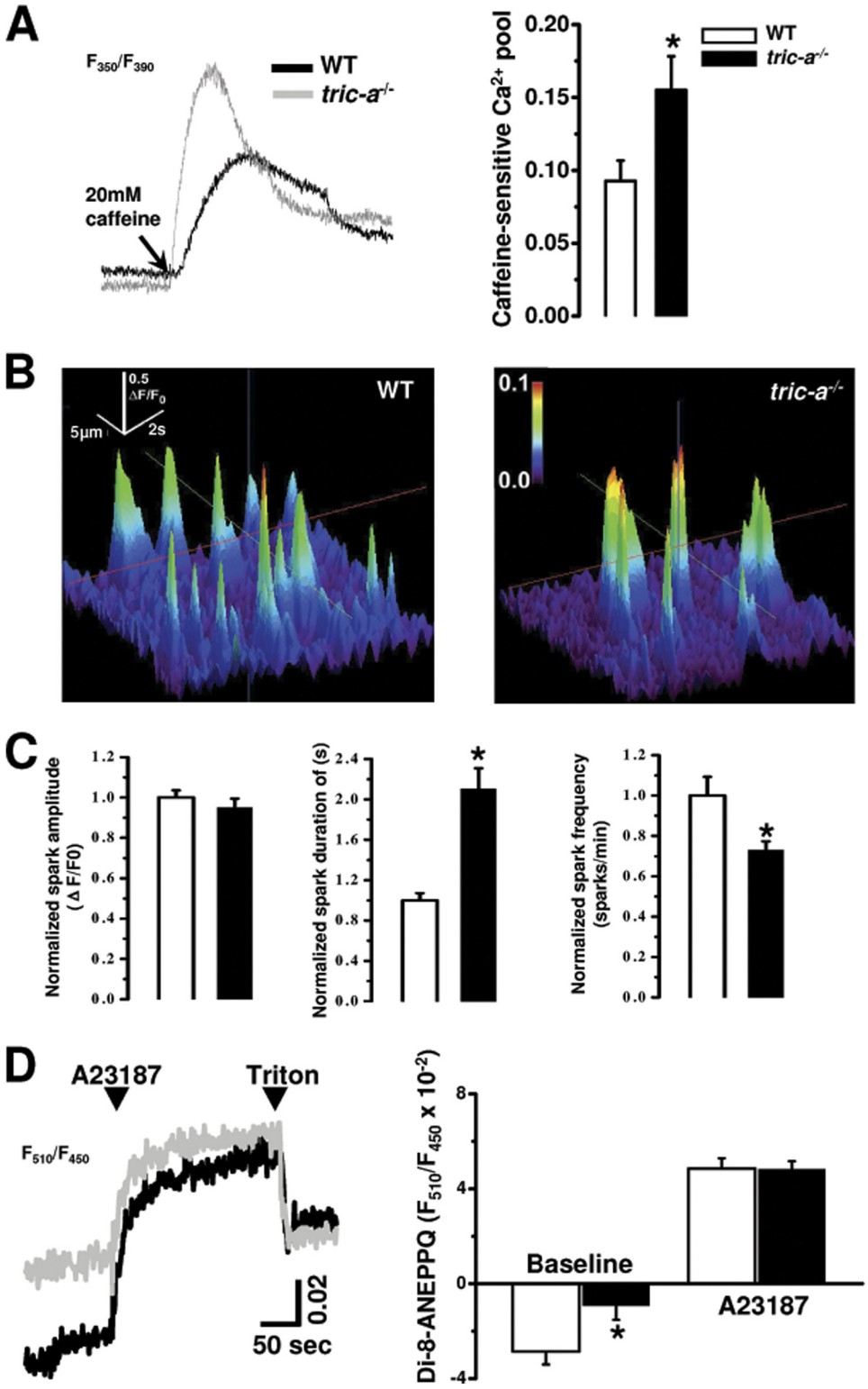

FIGURE 3. **Altered SR Ca^{2+} release properties and membrane potential in *tric-a* mutant muscles.** *A*, representative trace of intracellular Ca^{2+} transient induced by 20 mM caffeine (*arrow*) in FDB from wild type (*gray*) and *tric-a*$^{-/-}$ (*black*) mice (*left panel*). Fura-2 fluorescence was recorded at excitation wavelengths of 350 (F_{350}) and 380 nm (F_{380}). The peak caffeine response at F_{350}/F_{380} in wild type (*open bar*) and *tric-a*$^{-/-}$ muscle (*filled bar*) is summarized in the *right panel*, $n = 10$. *B*, representative three-dimensional images of Ca^{2+} spark in wild type and *tric-a*$^{-/-}$ FDB fibers. *C*, normalized amplitude ($\Delta F/F_0$), duration of single spark (ms), and frequency per min of osmotic-induced Ca^{2+} spark in FDB of the wild type (*open*) and *tric-a*$^{-/-}$ mice (*filled*) were summarized here, $n = 13$–24. The value of wild type fibers were set as 1. *D*, representative trace of SR membrane potential measurement by di-8-ANEPPQ dye at F_{510}/F_{450} (*left panel*) in SR vesicle isolated from wild type (*gray*) and *tric-a*$^{-/-}$ (*black*) mice, and *arrows* designate when A23187 (Ca^{2+} ionophore) and Triton were added (*left panel*). *Right panel* shows summarization of this data, F_{510}/F_{450} after addition of Triton was set as 0, $n = 6$. All values were mean ± S.E., *, $p < 0.05$.

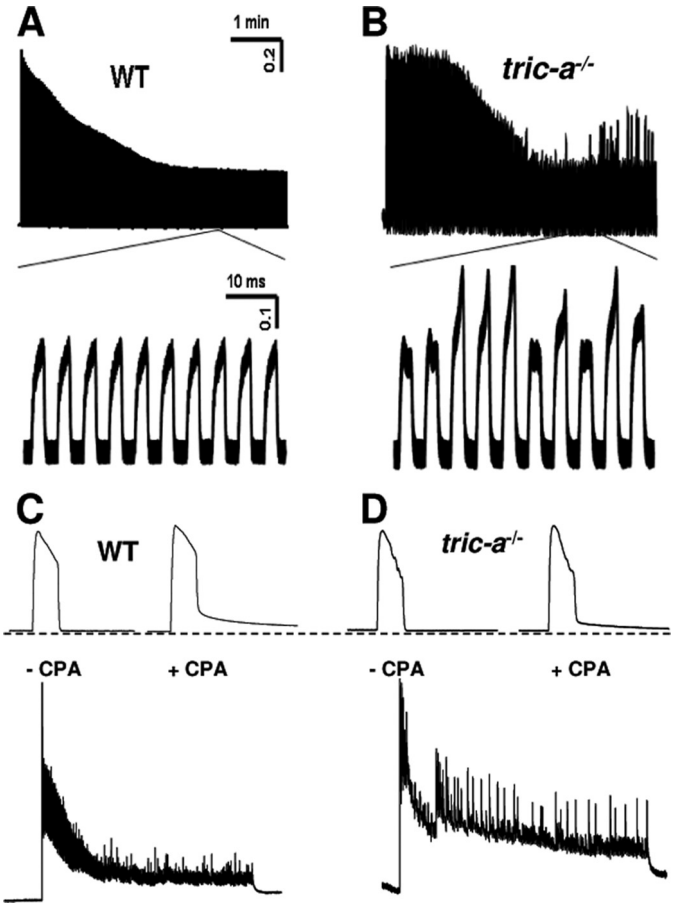

FIGURE 4. **Mechanical alternans in TRIC-A absent muscles induced by fatigue stimulation.** *A*, isolated muscle bundles from wild type mice show monotonic decrease in contractile force, when subjected to fatiguing stimulations by the 50% T_{max} frequency. *B*, isolated muscle bundles from the *tric-a*$^{-/-}$ mice show irregular patterns contractile force, when subjected to similar fatiguing stimulations as in *A*. Enlarged individual contractile forces shown in the *lower panels* reveal the appearance of alternans in the *tric-a*$^{-/-}$ muscle. *C*, EDL muscles from the wild type mice were treated with 20 μM CPA for 5 min, and tetanic contractile force measurements reveal the appearance of the characteristic slow relaxing phase (*top panel*). In the presence of CPA, fatiguing stimulation leads to the appearance of mild alternans in wild type muscle (*bottom panel*). The trace is representative of 4 of 10 muscle preparations. *D*, representative traces for the *tric-a*$^{-/-}$ muscle as shown using identical experimental conditions as in *C*. Clearly, CPA treatment leads to aggravation of alternan events in the *tric-a*$^{-/-}$ muscle. Trace shown at the *bottom panel* of *D* is representative of 8 of 10 muscle preparations tested.

muscle. Knock-out of *tric-a* leads to defects in SR membrane structure and membrane permeability, which may be associated with the compromised Ca^{2+} spark signaling in the *tric-a*$^{-/-}$ muscle. The irregular mechanical alternans in the mutant muscle is likely due to instability in Ca^{2+} movement across the SR membrane. These findings suggest that TRIC-A is an important regulating moiety for the Ca^{2+} release event in skeletal muscle. Our data should provide insights for further investigating the mechanisms of skeletal muscle E-C coupling process under physiological and pathophysiological conditions.

Acknowledgment—We thank Dr. Takahiro Iwamoto for providing antibodies to Na^+-Ca^{2+} exchanger subtypes.

REFERENCES

1. Ríos, E., Ma, J. J., and González, A. (1991) *J. Muscle Res. Cell Motil.* **12,** 127–135
2. Melzer, W., Herrmann-Frank, A., and Lüttgau, H. C. (1995) *Biochim. Biophys. Acta* **1241,** 59–116
3. Fill, M., and Copello, J. A. (2002) *Physiol. Rev.* **82,** 893–922
4. Takeshima, H., Komazaki, S., Nishi, M., Iino, M., and Kangawa, K. (2000) *Mol. Cell* **6,** 11–22
5. Hirata, Y., Brotto, M., Weisleder, N., Chu, Y., Lin, P., Zhao, X., Thornton, A., Komazaki, S., Takeshima, H., Ma, J., and Pan, Z. (2006) *Biophys. J.* **90,** 4418–4427
6. Yazawa, M., Ferrante, C., Feng, J., Mio, K., Ogura, T., Zhang, M., Lin, P. H., Pan, Z., Komazaki, S., Kato, K., Nishi, M., Zhao, X., Weisleder, N., Sato, C., Ma, J., and Takeshima, H. (2007) *Nature* **448,** 78–82
7. Pitt, S. J., Park, K. H., Nishi, M., Urashima, T., Aoki, S., Yamazaki, D., Ma, J., Takeshima, H., and Sitsapesan, R. (2010) *Biophys. J.* **99,** 417–426
8. Coronado, R., and Miller, C. (1980) *Nature* **288,** 495–497
9. Yamazaki, D., Komazaki, S., Nakanishi, H., Mishima, A., Nishi, M., Yazawa, M., Yamazaki, T., Taguchi, R., and Takeshima, H. (2009) *Development* **136,** 2355–2361
10. Saito, A., Seiler, S., Chu, A., and Fleischer, S. (1984) *J. Cell Biol.* **99,** 875–885
11. Wang, X., Weisleder, N., Collet, C., Zhou, J., Chu, Y., Hirata, Y., Zhao, X., Pan, Z., Brotto, M., Cheng, H., and Ma, J. (2005) *Nat. Cell Biol.* **7,** 525–530
12. Zhao, X., Yoshida, M., Brotto, L., Takeshima, H., Weisleder, N., Hirata, Y., Nosek, T. M., Ma, J., and Brotto, M. (2005) *Physiol. Genomics* **23,** 72–78
13. Weisleder, N., Takeshima, H., and Ma, J. (2008) *Cell Calcium* **43,** 1–8
14. Lai, F. A., Erickson, H. P., Rousseau, E., Liu, Q. Y., and Meissner, G. (1988) *Nature* **331,** 315–319
15. Fleischer, S., and Inui, M. (1989) *Annu. Rev. Biophys. Biophys. Chem.* **18,** 333–364
16. MacLennan, D. H. (1990) *Biophys. J.* **58,** 1355–1365
17. Surawicz, B., and Fisch, C. (1992) *J. Am. Coll. Cardiol.* **20,** 483–499
18. Weiss, J. N., Karma, A., Shiferaw, Y., Chen, P. S., Garfinkel, A., and Qu, Z. (2006) *Circ. Res.* **98,** 1244–1253
19. Laurita, K. R., and Rosenbaum, D. S. (2008) *Prog. Biophys. Mol. Biol.* **97,** 332–347
20. Eisner, D. A., Li, Y., and O'Neill, S. C. (2006) *Heart Rhythm.* **3,** 743–745
21. Wilson, L. D., Wan, X., and Rosenbaum, D. S. (2006) *Ann. N.Y. Acad. Sci.* **1080,** 216–234
22. Li, Y., Díaz, M. E., Eisner, D. A., and O'Neill, S. (2009) *J. Physiol.* **587,** 1283–1292
23. Jiang, D., Xiao, B., Yang, D., Wang, R., Choi, P., Zhang, L., Cheng, H., and Chen, S. R. (2004) *Proc. Natl. Acad. Sci. U.S.A.* **101,** 13062–13067
24. Kong, H., Wang, R., Chen, W., Zhang, L., Chen, K., Shimoni, Y., Duff, H. J., and Chen, S. R. (2007) *Biophys. J.* **92,** 2757–2770
25. Landeira-Fernandez, A. (2001) *J. Exp. Biol.* **204,** 909–921
26. Huchet, C., and Léoty, C. (1994) *Can. J. Physiol. Pharmacol.* **72,** 833–840